



Ion exchange: an essential piece in the fabrication of zeolite adsorbents

Cite this: DOI: 10.1039/d5cp00894h

 Chenxin Li,^a Tiesen Li,^b Qingyan Cui,^a Tinghai Wang,^a Chan Wang,^a Jiao Yang,^b Jie Shi,^b Xiaojun Bao^b and Yuanyuan Yue^b

Adsorptive separation, which relies on the size, polarity, and affinity of guest molecules, is an efficient, eco-friendly, and cost-effective method. Zeolite-based adsorbents, known for their uniform pore size and regenerability, have exhibited exceptional performance in many challenging adsorption processes, such as the separation of *n*-paraffin/*i*-paraffin and xylene isomers. Ion exchange, as an essential piece in the fabrication of zeolite-based adsorbents, significantly affects overall performance. In this review, we survey the recent key developments and issues within ion exchange research of zeolite-based adsorbents, including the solution pH, solution concentration, ion-exchange cycles, ion-exchange temperature, ion-exchange time, calcination temperature, and discuss the mechanisms of their influence on zeolite adsorption. This review also elaborates on the negative effects of improper ion exchange on incomplete cation exchange, cation migration, collapse of the zeolite structure, and blockage of zeolite pores. Other parameters that lack research but have been proven to affect ion exchange are also mentioned. We hope to generate interest in the wider community and encourage others to make use of ion exchange in tackling challenges of adsorption separation science and engineering.

 Received 6th March 2025,
 Accepted 4th June 2025

DOI: 10.1039/d5cp00894h

rsc.li/pccp

1. Introduction

Adsorption is a cost-effective and efficient separation method widely utilized for separating chemicals that are difficult to separate using traditional distillation techniques.¹ Zeolite adsorbents, known for their uniform pore size and regenerability, have been successfully employed in various industrial applications, including gas drying, oxygen production, hydrogen production, CO₂ separations, and the separation of *n*-paraffins from *i*-paraffins and xylene isomers.² In 2022, zeolites accounted for approximately 40% of the adsorbents market and are projected to experience a compound annual growth rate of 6.1% from 2023 to 2033.³

Zeolite, which is a classic inorganic porous material featured with exceptional stability, high adsorptive capacity, tuneable adsorption selectivity, and low production cost, has been seen as an excellent and practical adsorbent. Zeolite adsorbents are usually aluminosilicates,⁴ whose frameworks are constructed by corner-sharing of TO₄ (T = Si and Al) tetrahedra. These frameworks have considerable stability and offer abundant uniform pores to store guest molecules (adsorbates). In order to balance the negative charges from the framework AlO₄ tetrahedra, there are some framework and extra-framework

cations located in the zeolite pores, which significantly affect the adsorption selectivity of zeolites. The selective adsorption capacity of zeolites is typically attributed to four major effects: steric effect, equilibrium effect, kinetic effect, and trapdoor effect.⁵ All of these effects are related to the counter cations within zeolites, meaning that the adsorption selectivity of zeolites can be improved by altering the counter cations.

Ion exchange is a common, simple, and valuable method to introduce specific cations into zeolites.⁶ Numerous zeolite adsorbents are fabricated through this process. For example, 3A and 5A zeolites, which are K- and Ca-exchanged forms of zeolite A, respectively, have been widely used in gas drying, air separation, hydrogen purification, and paraffin isomer separation.⁷ Additionally, Li- and Ba-exchanged zeolite X demonstrate impressive adsorptive performance in oxygen purification⁸ and *p*-xylene purification,⁹ respectively. The growing demand for zeolite adsorbents with high selectivity for specific chemicals has led to the continuous development and reporting of novel zeolite adsorbents.¹⁰ Currently, a large amount of research has explored the exchange of almost all alkali metals and alkaline earth metals in zeolites,¹¹ but improper ion exchange operations would decrease zeolite adsorption performance. Based on the mechanisms of adsorptive separation in zeolites,⁵ those with a high degree of ion exchange, optimal cation distribution, and large surface area typically exhibit remarkable selective adsorption properties. As illustrated in Fig. 1, there are four key issues during the ion exchange process that can affect the adsorption

^a National Engineering Research Center of Chemical Fertilizer Catalyst, College of Chemical Engineering, Fuzhou University, Fuzhou 350002, P. R. China.
 E-mail: litiesen@fzu.edu.cn, yueyy@fzu.edu.cn

^b Qingyuan Innovation Laboratory, Quanzhou 362801, Fujian Province, P. R. China

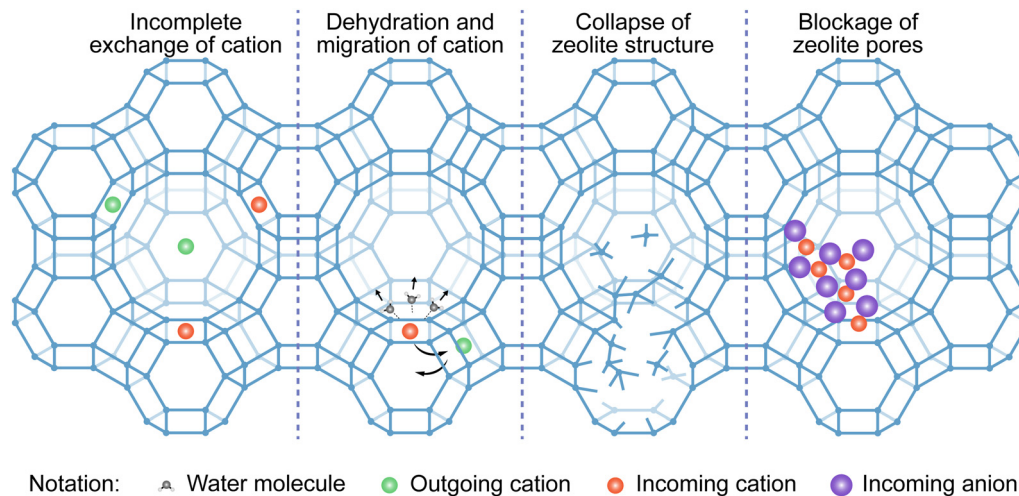


Fig. 1 Schematic illustration of four major issues in ion exchange of zeolite.

capabilities of zeolites: incomplete cation exchange,¹² cation migration,¹³ collapse of zeolite structure,¹⁴ and blockage of zeolite pores.¹⁵

Complete cation exchange is beneficial for adsorption,^{12,16} as incoming cations provide interaction sites for adsorbate molecules. However, achieving this in some ion exchange systems is challenging. Once cations enter the zeolite, they randomly distribute among various cation sites, but only those in specific locations can effectively interact with adsorbate molecules.^{17–19}

Additionally, the zeolite pores play a crucial role in its adsorption properties, providing channels for adsorbates to diffuse and interact with cations. The pores are formed by the zeolite framework, meaning that pore integrity is compromised if the framework collapses. During ion exchange, the framework may be damaged due to hydrolysis and thermal vibrations.^{20,21} Moreover, pore blockage can occur when cations and anions are absorbed into the pores after cation exchange, a phenomenon known as salt imbibition,²² leading to undesirable pore obstruction.¹⁵

Therefore, the impact of ion exchange on zeolite adsorption performance is determined by factors such as the degree of ion exchange, cation migration, the integrity of the zeolite framework, and pore blockage. These criteria are essential for understanding the mechanisms of ion exchange in zeolite adsorption.

Given the importance of ion exchange in the separation performance of zeolites, we provide a brief review of the factors influencing the ion exchange process and explore how these factors affect the adsorption performance of zeolites. We mainly focus on the parameters of solution pH, solution concentration, ion exchange cycles, ion exchange temperature, ion exchange time, and calcination temperature. These variables play a crucial role in influencing the ion exchange process, and their mechanisms have been extensively researched.

To avoid redundancy, we discuss the impact of these variables on zeolite adsorption performance through the four mentioned criteria, including the degree of ion exchange,

cation migration, the integrity of the zeolite framework, and pore blockage within the zeolite. These discussions emphasize the connections between the four criteria and the parameters of ion exchange, rather than directly relating these variables to the adsorption capacity of zeolite. Based on these connections, tailored suggestions are presented to optimize the ion exchange process of zeolites. Furthermore, other parameters that have not been adequately researched but have demonstrated effects on ion exchange are also discussed.

2. Fundamental principles of ion exchange in zeolite

Although most cations can move freely within the zeolite channels and the external solution, the “anions” inside the zeolite cannot move freely as they are part of the zeolite framework. However, both cations and anions in the external solution can move freely. Namely, while anions in aqueous solution can theoretically move into and out of the zeolite freely, the anionic framework of the zeolite cannot do the converse with respect to the solution phase. Therefore, anions in the solution can only enter the zeolite when accompanied by an equivalent amount of cations; otherwise, it would violate the requirement of charge neutrality in each phase. This raises an important question: how is the ion exchange process in zeolites actually achieved?

The details of cation exchange in zeolite, which are pictured in Fig. 2, can be described as follows: (1) the incoming cations are dissociated in water to become hydrated cations; (2) the incoming cations, accompanied by water molecules, diffuse from the external solution into the zeolite pores; (3) the incoming cations exchange with the outgoing cations in the zeolite pores; (4) the outgoing cations diffuse from the zeolite pores into the external solution; (5) an ion exchange equilibrium is achieved between the zeolite and the solution.

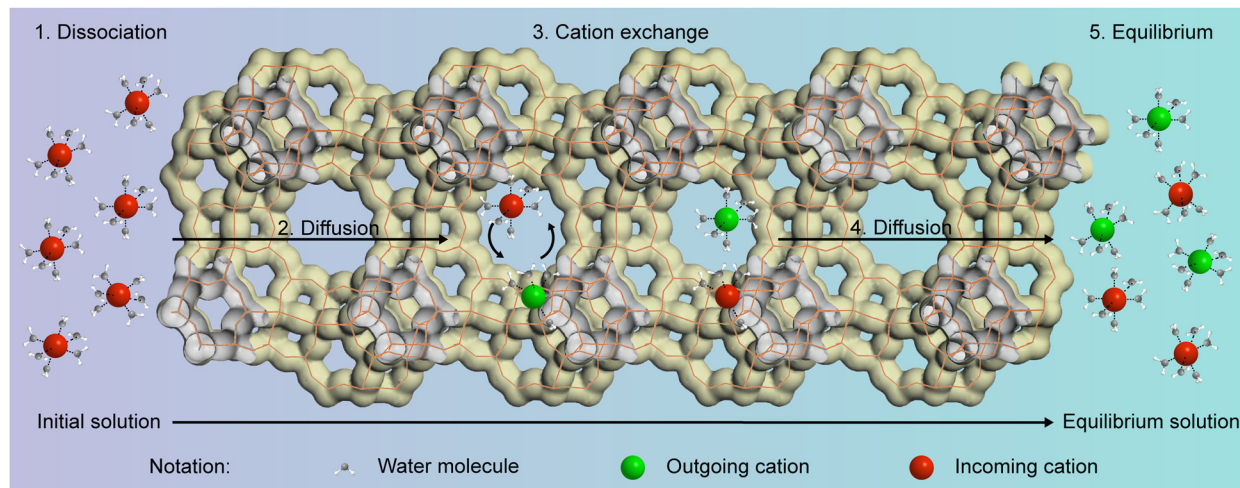


Fig. 2 Schematic overview of fundamental principles of ion exchange in zeolite.

The ion exchange equilibrium can be described by the following equation:²³



Here, A and B are the incoming and outgoing cations, with a and b denoting the valencies of cations A and B, while the subscripts “(zeo)” and “(sol)” refer to the ions being either inside the zeolite or in the solution. Based on this equation, the concept of the degree of ion exchange (DE) in this paper is defined as:

$$\text{DE} = \frac{(m_{B0} - m_{B1})}{m_{B0}} \times 100\% \quad (2)$$

Where m_{B0} and m_{B1} stand for the molalities of cation B in the zeolite before and after ion exchange. The degree of ion exchange is calculated based on the molality of the outgoing cation instead of the incoming cation because the molality of the incoming cation is affected by ion exchange and salt imbibition simultaneously. When salt imbibition occurs, the degree of ion exchange calculated based on the molality of the incoming cation may be overestimated. In contrast, the cation loading is calculated based on the molality of the incoming cation, which reveals the real content of the incoming cation in the zeolite.

If zeolites are exposed to a series of isonormal solutions containing different incoming and outgoing cations under standard conditions of temperature and pressure, an ion exchange isotherm can be constructed to obtain information on the cation distribution between the zeolite and the solution phase. We can plot an isotherm to record the equivalent fraction S_A of the incoming cations in solution and their equivalent fraction Z_A in the zeolite. These fractions reflect the proportion of the exchange capacity in each phase and can be expressed in binary ion exchange as follows:

$$Z_A = \frac{am_A}{am_A + bm_B} \quad (3)$$

$$S_A = \frac{an_A}{an_A + bn_B} \quad (4)$$

Here, subscript “A” and “B” refer to cations A and B, with a and b representing the valencies of exchanging cations A and B, while m and n indicate the molalities of cations in the zeolite and solution phases, respectively.

The idealized shape of the ion exchange isotherm for zeolites is shown in Fig. 3.²⁴ This shape illustrates the relative preferences of cations between the solid zeolite and the solution. When the zeolite has equal affinity for two cations, the isotherm appears as a straight line, represented by the dashed line in Fig. 3. When cation A readily displaces cation B from the zeolite, the isotherm resembles curve (i). Conversely, if cation A remains in solution and does not easily displace cation B from the zeolite under the experimental

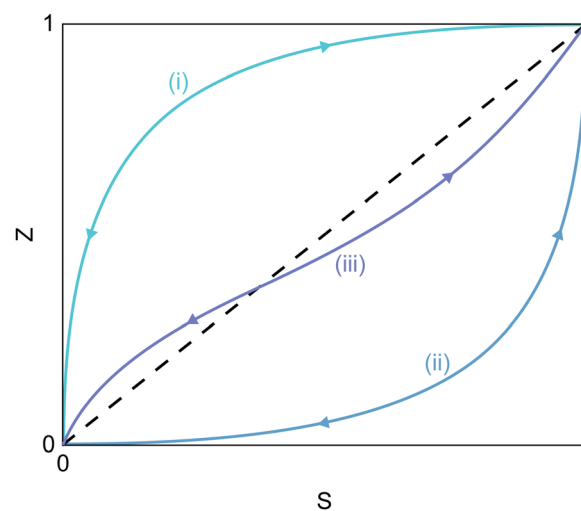


Fig. 3 Idealized cation exchange isotherms. Dashed line: non-selective exchange; curve (i) selective exchange for incoming cations; curve (ii) unselective exchange for incoming cations; curve (iii) a change in selectivity as a function of S .

temperature and concentration conditions, the isotherm takes the shape shown as curve (ii). When selectivity changes occur within the studied concentration range, an S-shaped curve appears as shown as curve (iii), indicating that the zeolite has multiple exchange sites available for competing cations.

The ion exchange process in zeolite can be considered a chemical reaction, as mentioned in eqn (1). The relationship between its thermodynamic equilibrium constant K_a and the concentration of each species can be described as follows:²⁵

$$K_a = \frac{f_A^b Z_A^b \gamma_B^a n_B^a}{f_B^a Z_B^a \gamma_A^b n_A^b} \quad (5)$$

Let f_A and f_B represent the rational single-ion activity coefficients of ions A and B in the zeolite phase, while γ_A and γ_B denote the molal single-ion activity coefficients of ions A and B in the solution phase. Z_A and Z_B refer to the equivalent fractions of ions A and B in the zeolite phase, and n_A and n_B are the molalities of ions A and B in the solution phase. Although the molal single-ion activity coefficients can vary with the degree of ion exchange,²² their values remain greater than zero.

To calculate the thermodynamic equilibrium constant of ion exchange, it is common to define a function K_c

(known as the corrected selectivity quotient²⁶), which is related to K_a :

$$K_c = K_a (f_B^a / f_A^b) \quad (6)$$

Generally, the thermodynamic equilibrium constant K_a can be determined using the Gaines and Thomas equation:²⁷

$$\ln K_a = (b - a) + \int_0^1 \ln K_c dZ_A \quad (7)$$

However, in reality, changes in water activity within the zeolite framework and salt imbibition may alter the thermodynamic equilibrium constant. When these phenomena cannot be ignored, corresponding functions should be added to the equation:

$$\ln K_a = (b - a) + \int_0^1 \ln K_c dZ_A + \Delta + \Psi \quad (8)$$

Here, Δ represents a composite factor that accounts for alterations in both the quantity and activity of water within the exchanger, reflecting differences in external electrolyte concentration and the zeolite composition, and ψ is a function that takes salt imbibition into account (see ref. 26 for more details).

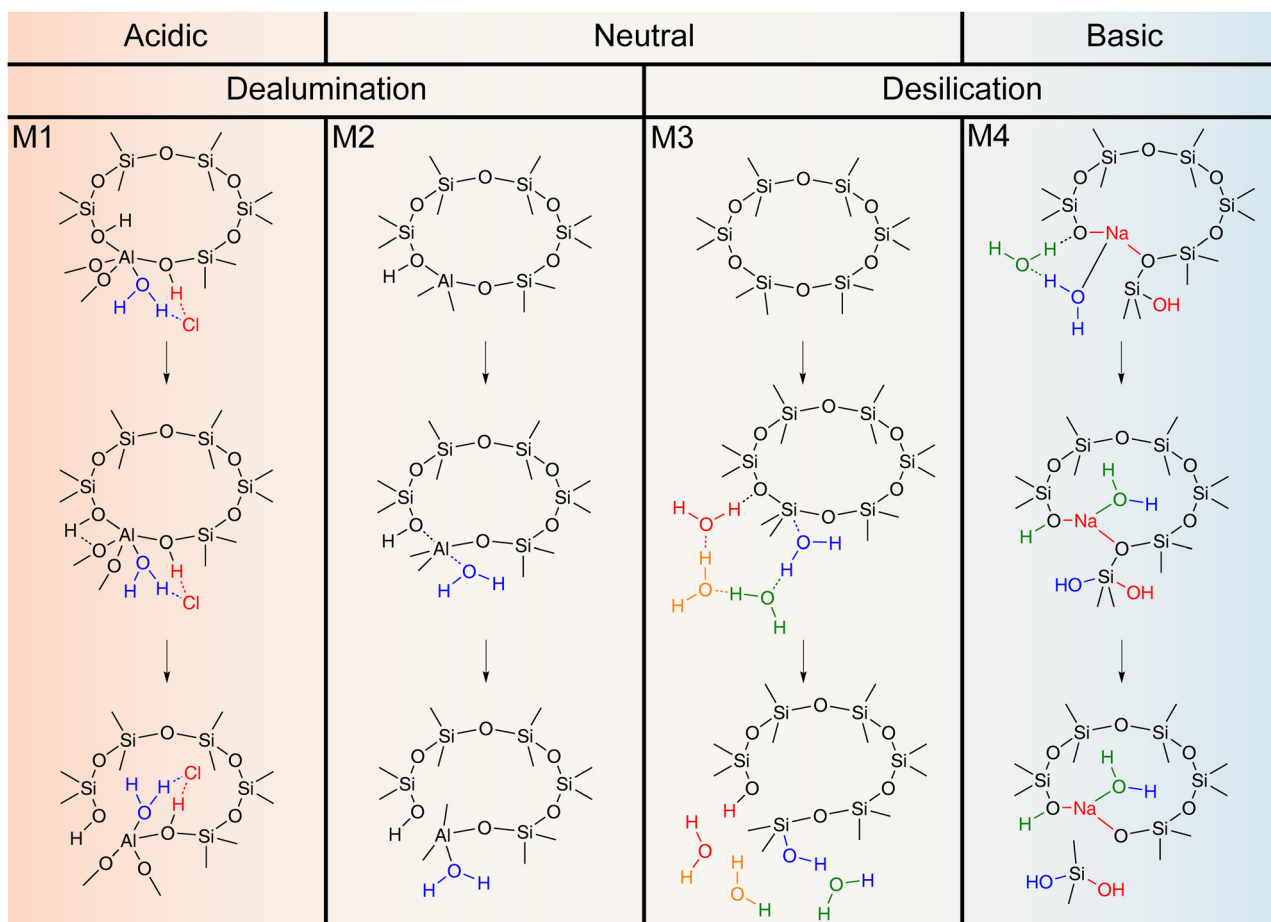


Fig. 4 Schematic overview of zeolite hydrolysis mechanism under acidic, neutral and basic conditions. M1: dealumination in acidic conditions;³² M2: dealumination in neutral conditions;³³ M3: desilication in neutral conditions;³³ M4: desilication in basic conditions.³⁵

3. Effect of solution pH

For a specific zeolite, effective adsorption performance relies on two key factors: the integrity of the zeolite framework, which ensures the availability of sufficient effective adsorption sites, and the type of extra-framework cations, which typically alter the zeolite's pore structure or enhance its selectivity for specific molecules. The above two factors are significantly influenced by the pH of the ion exchange solution.

During the ion exchange process, both zeolites and incoming cations can undergo hydrolysis in aqueous solutions. Zeolite hydrolysis can cause structural damage,²⁸ while cation hydrolysis may hinder the effective entry of cations into the zeolite pores.²⁹ To minimize these hydrolytic effects, it is crucial to control the solution pH, as these reactions are undesirable. The mechanism of zeolite hydrolysis, detailed in Fig. 4, varies with the pH of the ion exchange solution.

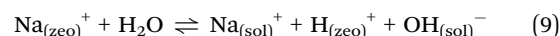
In acidic environments, zeolite hydrolysis primarily proceeds through dealumination reactions.^{30,31} Therefore, we only focus on the mechanism of Al–O bond cleavage promoted by the acid medium. This mechanism is denoted as M1 and is shown in Fig. 4. In this process, HCl molecules provide an acidic environment and act as catalysts to accelerate zeolite hydrolysis.³² The proton of HCl is positioned at a bridging oxygen near another OH-bridging (located at the Al–O₄ bond) that had been established before the introduction of HCl. At the same time, a single water molecule is adsorbed on the aluminum, resulting in the distance of the Al–O₄ bond being enlarged until it breaks.

Even under neutral conditions, water molecules act as nucleophiles to attack the silicon or aluminum of the zeolite framework, and thereby promoting partial and reversible hydrolysis. Heard *et al.* proved that zeolite could be hydrolyzed under milder aqueous conditions and revealed the mechanisms of the Al–O and Si–O bonds breaking, which are denoted as M2 and M3 in Fig. 4, respectively.³³ In M2, due to a Brønsted proton located in the bridging oxygen of the Si–O–Al bond, there is no requirement to introduce more water molecules for proton transfer to facilitate Al–O bond scission. After the aluminum absorbs a water molecule, it is easy for the Al–O bond to break. In M3, apart from the attacking water molecule, there are three other water molecules participating in the reaction. These additional water molecules transfer a proton from the attacking water to the axial framework oxygen *via* the Grotthuss mechanism to promote the Si–O bond breaking. Compared to the Si–O bond, the Al–O bond can break faster, because the energy barrier of Al–O bond scission is lower than that of Si–O bond scission. However, the hydrolysis products of Si–O–Si bond cleavage are slightly more stable based on thermodynamic analysis. Therefore, it is difficult to conclude which hydrolysis mechanism plays a leading role in neutral conditions.

In basic environments, it is generally believed that the desilication reaction plays a dominant role in zeolite hydrolysis.^{34,35} During the desilication process, basic molecules can serve as a reactant³⁶ or a catalyst.³⁵ Taking the NaOH molecule as an example, Jin *et al.* suggested that NaOH could act as a reactant in the desilication reaction only under the conditions in which

there was a local excess of NaOH and little water.³⁵ Therefore, they proposed another mechanism that was more suitable for zeolite hydrolysis under aqueous basic conditions. This mechanism is denoted as M4 in Fig. 4. In this process, there is one NaOH molecule and two water molecules participating in the reaction. One water molecule, whose oxygen binds to the Na⁺ cation, provides a hydroxyl group and a proton; the other water molecule is used to transfer the proton. Finally, the Si–O–Si bond is broken, which binds to the Na⁺ cation.

It should be noted that the models of these dealumination mechanisms are protonic zeolites, including M2 and M3 mechanisms. It does not mean that the aluminum in cationic zeolites cannot be hydrolyzed, but protonic zeolites more easily achieve dealumination with respect to cationic zeolites. Sun *et al.* used DFT calculations to successfully prove that the first Al–O bond in H-LTA zeolite was easier to break than in cationic LTA zeolite.³⁷ The minimal activation energies of the first Al–O bond scission in H-LTA and Na-LTA zeolites were 75 and 118 kJ mol⁻¹, respectively.³⁷ Therefore, the outgoing cations within the zeolite probably exchange with protons from water dissociation before zeolite dealumination. Taking sodium zeolite as an example, the reaction equation can be expressed as:



Where the subscripts “(zeo)” and “(sol)” refer to the ions being either inside the zeolite or in the solution, respectively. Eqn (9) illustrates that elevating the hydroxide ion concentration diminishes the ingress of hydrated hydrogen ions into the zeolite, implying that raising the solution's pH value can decelerate the zeolite's dealumination rate.

Enhancing the solution's pH value can reduce zeolite dealumination, but it may promote zeolite desilication based on mechanism M4. Therefore, in order to reduce zeolite hydrolysis, it is crucial to adjust the pH of the ion exchange solution to balance the adverse impacts of dealumination and desilication on zeolite structural stability.

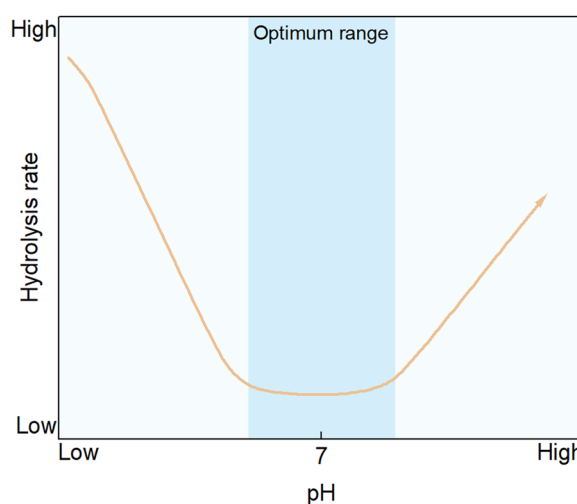


Fig. 5 The conjectural relationship between the rate of zeolite hydrolysis and the pH of the ion exchange solution.

Generally, there exists an optimum pH range that minimizes the rate of zeolite hydrolysis, as illustrated in Fig. 5. This optimum range typically lies near neutral pH. Cama *et al.* investigated the dissolution rate of NaP1 zeolite at various pH values in the range of 2–12.³⁸ Their results showed that dissolution rates decreased with increasing pH under acidic conditions, but increased under basic conditions, with the slowest rates observed at near neutral pH (6.5–9.5). A similar trend was reported by Ragnarsdóttir,³⁹ who found that the dissolution of heulandite was accelerated in both acidic and basic environments, with a minimum dissolution rate at pH 7.2.

The precise optimum pH range for minimizing zeolite hydrolysis depends on the nature of the zeolite,^{33,39,40} especially the Si/Al ratio.³¹ In general, zeolites with higher framework aluminum species exhibit a higher optimal pH. Experimental studies on A-type zeolites (which have high framework aluminum species) confirm that such zeolites are more stable in weakly alkaline environments.^{40–42}

Although it is advantageous for zeolites to maintain their structural stability in near neutral environments, this doesn't mean that all ion exchange systems are suitable to operate under these environments. The hydrolysis of the incoming cations should not be ignored, as it can decrease the efficiency of cation exchange, and it is easily achieved in basic solutions.^{43,44} Apart from alkali metals and some alkaline-earth metals (strontium, barium), whose hydroxides can easily dissolve in water, most metal cations are readily hydrolyzed in basic or even neutral environments. Even though no metal precipitations occur, when cations hydrolyze, other hydrolyzed species will become the predominant metal species in water, such as MOH^+ , $\text{M}(\text{OH})_2$, and $\text{M}(\text{OH})_3^-$, which are more difficult to pass through small cages compared to free cations.⁴⁵ For example, Cd(II) exists primarily as Cd^{2+} at $\text{pH} \leq 8$; the $\text{Cd}(\text{OH})^+$ ion begins to form at $\text{pH} > 8$ and its contribution is important at pH 9; at pH 10.6, the majority of the cadmium is in the form of $\text{Cd}(\text{OH})_2$ with the remainder $\text{Cd}(\text{OH})^+$ and $\text{Cd}(\text{OH})_3^-$; finally the anion $\text{Cd}(\text{OH})_3^-$ is the predominant species at $\text{pH} > 13$ (Fig. 6).⁴⁶ Suzuki *et al.* investigated how pH affected the movement of Co^{2+} ions within zeolite Y.⁴⁷ They discovered that the Co^{2+} levels in the zeolite decreased as the pH exceeded 10.5. They suggested that it was difficult for Co^{2+} ions to enter the sodalite cages of zeolite Y, because some Co^{2+} ions associated with hydroxide ions and were blocked in the supercages of zeolite Y at pH 10.5. When the pH exceeded 10.7, the hydrolysis of Co^{2+} ions increased, causing them to preferentially remain in the supercages and outside the zeolite rather than in smaller cages.

Therefore, it is necessary to adjust the pH of the ion exchange solution to balance the influences of zeolite and cation hydrolysis. Weakly acidic conditions facilitate the migration of most metal cations, while weakly alkaline conditions help reduce the rate of zeolite hydrolysis. When cations are prone to hydrolysis in alkaline or even neutral conditions, ion exchange operations should ideally occur in a weakly acidic environment, particularly for transition metal cations. For instance, Sung *et al.* exchanged Ni^{2+} ions into zeolite Y in an aqueous solution of 0.05 M $\text{Ni}(\text{NO}_3)_2 \cdot 6\text{H}_2\text{O}$ at pH 4.9.⁴⁸ Bae and

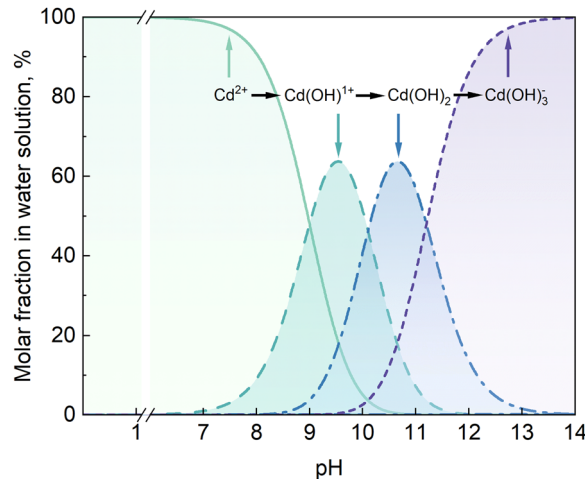


Fig. 6 Speciation diagrams of Cd(II) in water solutions at $T = 25\text{ }^\circ\text{C}$.⁴⁶

Seff introduced Zn^{2+} ions into zeolite X at pH 5.5 with a 0.05 M $\text{Zn}(\text{NO}_3)_2 \cdot 6\text{H}_2\text{O}$.⁴⁹ Firor and Seff exchanged Ni^{2+} and Fe^{2+} into zeolite A at pH values of 6.5.⁵⁰ In alkaline solutions, metals that can exist as free cations can be exchanged in mildly alkaline environments, which helps mitigate zeolite hydrolysis. For example, Zhang *et al.* adjusted the pH to 9 while preparing Na-CHA, K-CHA, and Li-CHA zeolites through ion exchange.⁵¹ Similarly, Hutson *et al.* set the pH to 9 for Li-LSX and Li-X zeolite preparation,⁵² while Liu *et al.* adjusted the pH to 12 for SrA zeolite preparation.⁵³ Although the optimal pH value for ion exchange, which differs depending on the type of zeolites, is challenging to predict, it can be determined through experimental methods.

4. Effect of solution concentration

During the ion exchange process, cations from the solution diffuse into the zeolite channels, where they exchange with outgoing cations and neutralize the negative charges of the zeolite framework. This diffusion process adheres to Fick's laws of diffusion,²² which can be expressed as:

$$J_i = -D_i \nabla c_i \quad (10)$$

Here, J is the flux, D is a diffusion coefficient, c stands for the concentration of species i , and ∇ refers to gradient. In eqn (10), it is evident that the flux increases with the concentration gradient. At the beginning of ion exchange, the concentration of species i in the zeolite is zero. Therefore, increasing the solution concentration is an effective way to enhance the concentration gradient. This indicates that a higher solution concentration can accelerate the diffusion of cations into the zeolite, facilitating the ion exchange process until equilibrium is achieved. In addition, a higher concentration can reduce the immersion time of the zeolite in the solution, thereby minimizing hydrolysis.

As indicated in eqn (3), Z_A (the equivalent fraction of ions A in the zeolite phase) can increase with m_A (the molality of ion A)

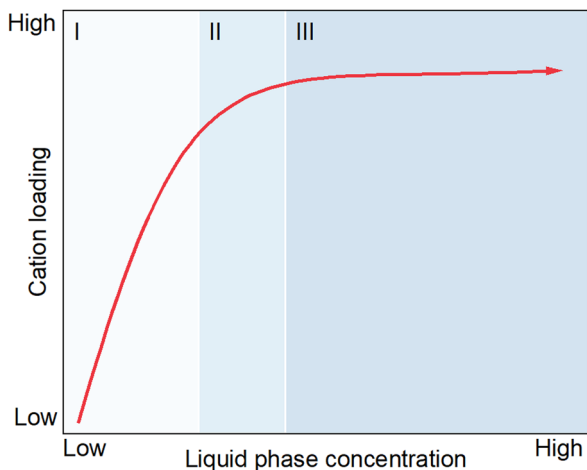


Fig. 7 Typical adsorption equilibrium isotherm. Region I: far from saturation; region II: approaching saturation; region III: saturated state.

until complete ion exchange occurs. This relationship is illustrated in Fig. 7,⁵⁴ which shows a typical adsorption equilibrium isotherm for ion exchange in zeolite.

A high concentration of the solution benefits both the kinetics and thermodynamics of the ion exchange process. However, it does not necessarily improve the adsorption performance of the zeolite. Once the ion exchange at the cation sites is complete, a high concentration may cause cations along with their corresponding anions to enter the zeolite, potentially obstructing its pores and reducing its adsorption capacity.^{15,55,56} For example, Liu *et al.* investigated Zn-exchanged Y zeolite for selective adsorption of benzene from benzene–cyclohexane mixture, and discovered that the adsorption performance of the zeolite was significantly influenced by the concentration of the ion exchange solution.⁵⁷ At a concentration of 0.05 M, the zeolite exhibited limited adsorption capacity and selectivity for benzene. As the concentration increased to 0.1 M, the zeolite demonstrated optimal adsorption capacity and improved selectivity. However, further increasing the concentration to 0.2 M led to a decrease in adsorption capacity, although selectivity continued to increase. When the concentration increased to 0.3 M, both adsorption capacity and selectivity were reduced. These results can be better understood by considering the isotherm of Zn²⁺ on NaY zeolite.⁵⁸ At initial concentrations below 0.06 M, the zinc uptake by the zeolite increased rapidly with increasing concentration, implying that a limited zinc content led to a reduced number of active sites available for benzene adsorption. At the concentration ranged from 0.06 M to 0.12 M, the Zn²⁺ loading approached saturation, suggesting most active sites were occupied, and resulting in improved adsorption capacity and selectivity. Once the concentration exceeded 0.12 M, the rate of zinc content uptake slowed, indicating that excess zinc salts began to fill the zeolite pores, ultimately leading to a decline in both the adsorption capacity and selectivity for benzene.

Based on these experimental phenomena and the mentioned theories of kinetics and thermodynamics, the adsorption equilibrium isotherm can be roughly categorized into three regions, which are shown in Fig. 7:

(1) Region I: the loading of incoming cations in zeolite increases rapidly with rising solution concentration, implying that the solution concentration of the incoming cation is too low to favor ion exchange in terms of kinetics and thermodynamics.

(2) Region II: the cation loading increases more slowly as the solution concentration rises, indicating that the cation loading is approaching saturation and the solution concentration is at a moderate level.

(3) Region III: changes in the cation concentration have little effect on the cation loading, suggesting that the cation loading reaches saturation and the zeolite pores are prone to blockage.

Therefore, when utilizing ion-exchanged zeolite for adsorption, it is crucial to control the concentration of the ion exchange solution to remain within region II. Maintaining a moderate concentration of the solution can help preserve the efficiency of ion exchange and prevent excessive cation accumulation, which can block the zeolite pores.

In order to obtain the adsorption equilibrium isotherm, the experimental data should be fitted to models of adsorption isotherms. Even though ion exchange is a unique form of adsorption, its adsorption equilibrium isotherm can often be fitted to common adsorption isotherm models, especially the Langmuir and Freundlich models.^{59–61} The Langmuir isotherm model is a monolayer adsorption model, assuming a homogeneous adsorbent surface with equal energy across all sorption sites.⁶² Its equation can be written as:

$$q_e = \frac{q_m K_L C_e}{1 + K_L C_e} \quad (11)$$

In this context, q_e represents the amount of adsorbate per unit of adsorbent mass at equilibrium, C_e is the concentration of adsorbate at equilibrium, q_m denotes the maximum saturated monolayer adsorption capacity of the adsorbent, and K_L is the Langmuir constant, which reflects the affinity between the adsorbent and adsorbate. The Freundlich isotherm, on the other hand, is a multilayer sorption model that assumes a heterogeneous sorbent surface.⁶³ Apart from ion exchange, the adsorption process may also involve complexation and multilayer sorption on the zeolite surface. Its equation can be written as:

$$q_e = K_F C_e^{1/n} \quad (12)$$

Where K_F represents the Freundlich isotherm constant, with n values ranging from zero to one, indicating the degree of surface heterogeneity or the intensity of adsorption.

Both the Langmuir and Freundlich equations have some limitations in practical applications. For instance, the Langmuir equation is only applicable to ideal monolayer adsorption scenarios, whereas the Freundlich equation can describe multilayer adsorption at low concentrations but may not be suitable at high concentrations. Furthermore, both equations do not account for intermolecular interactions and surface heterogeneity during the adsorption process. If Langmuir and Freundlich models do not adequately fit the experimental data, alternative models such as Dubinin–Radushkevich, Tempkin, Redlich–Peterson, Sips, and Toth isotherm models can be

considered.^{60,64,65} Fitting the adsorption equilibrium isotherm allows us to predict the relationship between solution concentration and cation loading. This understanding helps control the degree of ion exchange and prevent excessive cation loading, which may lead to the obstruction of zeolite pores.

5. Effect of ion exchange cycles

If a single ion exchange cycle with zeolite does not achieve the desired degree of ion exchange, additional cycles should be performed to improve the exchange efficiency. Although few studies directly investigate the impact of ion exchange cycles on the degree of ion exchange, we can predict this influence by analyzing the ion exchange isotherms.

In multi-cycle ion exchange, renewing the ion exchange solution increases S , which in turn affects Z . The influence of ion exchange cycles on the degree of exchange can be categorized into four types of isotherms.

The first type, shown by curve a in Fig. 8,⁶⁶ indicates that the preferences of incoming and outgoing cations for the zeolite are similar. Therefore, the degree of ion exchange can increase with each cycle until both S and Z reach 1.0.

The second type, represented by curve b in Fig. 8,⁶⁶ demonstrates that the zeolite has a significantly higher selectivity for incoming cations compared to outgoing ones. In this case, complete exchange of the cation can occur without S needing to equal 1.0, allowing the zeolite to achieve a high degree of ion exchange in just a few cycles.

The third type, represented by curve c in Fig. 8,⁶⁶ reveals that the zeolite's selectivity for incoming cations is much lower than that for outgoing cations. Achieving a relatively high degree of ion exchange requires more cycles, and complete exchange of the incoming cation is rarely attained, even though S equals 1.0.

The fourth type, shown by curve d in Fig. 8,⁶⁷ indicates that outgoing cations cannot be completely exchanged by incoming

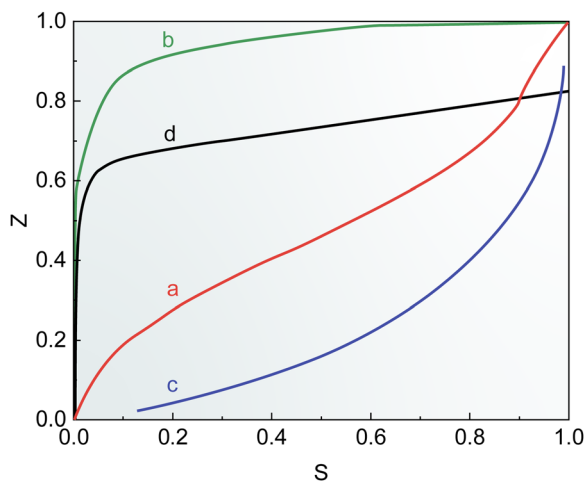


Fig. 8 The ion exchange isotherm of NaX zeolite with K^+ (red curve a),⁶⁶ Ag^+ (green curve b),⁶⁶ Li^+ (blue curve c),⁶⁶ Ba^{2+} (black curve d),⁶⁷ respectively, at 0.1 total normality and 25 °C.

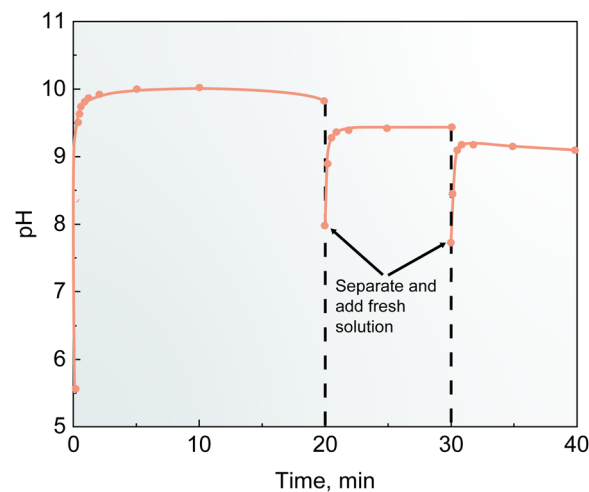


Fig. 9 Kinetic pH responses of zeolite after immersion in a 0.1 M sodium nitrate solution, illustrating the effects of repeated treatment with fresh solution.⁶⁸

cations. Here, selectivity is not the limiting factor; rather, size or volume exclusion prevents incoming cations from entering certain small zeolite cages or channels where cations are already present. Consequently, even with an infinite number of ion exchange cycles, the ion exchange level will stabilize at a certain value determined by the number of inaccessible cation sites for the incoming cations.

In addition to affecting the degree of ion exchange, the number of ion exchange cycles may also impact the structural stability of zeolite. As mentioned earlier, zeolite can hydrolyze in water, which raises the pH of the solution according to eqn (9). Hence, an increase in solution pH serves as evidence of zeolite hydrolysis. Townsend *et al.* observed that when zeolite was immersed in an aqueous solution, the pH initially increased with time before stabilizing at equilibrium.⁶⁸ If the zeolite was separated from the solution and placed into fresh solution, the pH would exhibit a similar pattern (Fig. 9).⁶⁸ This means that renewing the ion exchange solution promotes zeolite hydrolysis.

6. Effect of ion exchange temperature

As previously mentioned, ion exchange is a chemical reaction whose equilibrium is influenced by temperature. Generally, the standard enthalpy ΔH^0 of a reaction indicates whether heating can enhance it: if $\Delta H^0 > 0$, the reaction is endothermic and can be promoted by heating; if $\Delta H^0 < 0$, the reaction is exothermic and can be inhibited by heating. However, during the ion exchange process of zeolite, other reactions also affect cation loading and the overall standard enthalpy, including cation hydration and dehydration. Notably, the level of cation hydration decreases with increasing ion exchange temperature, while the energy required for cation dehydration rises with reduced hydration.⁶⁹ Once the hydrated incoming cation sheds its hydration shell, it becomes easier for the cation to enter the narrow cation sites within the zeolite framework,^{67,70} altering interactions with framework oxygens.⁷¹ Consequently, the

standard enthalpy of the entire ion exchange process varies with temperature⁷² and is not necessarily monotonic.⁷¹ Consequently, it is challenging to determine whether heating facilitates ion exchange in zeolite by measuring the standard enthalpy.

Fortunately, a straightforward method exists to directly distinguish whether high temperatures promote ion exchange in zeolite. This involves measuring the ion exchange isotherm at different temperatures. If any changes occur in the isotherm, as listed below, it indicates that high temperatures can indeed enhance ion exchange in zeolite:

(1) Complete ion exchange in zeolite cannot occur at low temperatures; increasing the temperature enhances the maximum degree of ion exchange (Fig. 10(a) and (b));

(2) Regardless of whether complete ion exchange is achievable, the maximum degree of ion exchange can be achieved at lower incoming cation equivalent fractions (S_A) after an increase in temperature (Fig. 10(c) and (d)).

The diffusion of cations within zeolite pores follows Fick's laws of diffusion, with Fick's first law described in eqn (10). In the equation, the diffusion coefficient D is temperature-dependent. For cation self-exchange, if a linear relationship can be established between the natural logarithm of the diffusion coefficient ($\ln D$) and the inverse of the temperature (T^{-1}), this relationship can be described using the Arrhenius equation:

$$D_{AA} = D_{AA}^0 \exp(-E_a/RT) \quad (13)$$

Where D_{AA} is the self-diffusion coefficient of cation A, D_{AA}^0 is the pre-exponent factor, E_a is the activation energy, R is the gas constant ($8.314 \text{ J (mol K)}^{-1}$), and T is the ion exchange temperature. Within a specific temperature range, D_{AA}^0 and E_a can be considered as constants independent of temperature. As shown in eqn (13), the self-diffusion coefficient D_{AA} increases with temperature.^{73–76} Outside this range, D_{AA}^0 and E_a may vary due to factors such as changes in the cation hydration radius, cation diffusion pathways, and interactions between cations and zeolite frameworks.⁷⁷

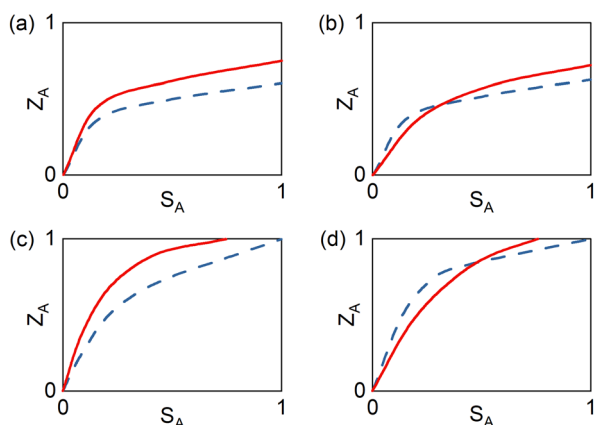


Fig. 10 Changes in the ion exchange isotherm indicate that ion exchange of zeolite has been promoted. The red solid line represents data at high temperature, while the blue dashed line represents data at low temperature.

Although D_{AA}^0 and E_a may fluctuate with temperature, higher temperatures consistently enhance the cation diffusion rate, regardless of the rate-controlling step.⁷⁸ Furthermore, the values of D_{AA}^0 and E_a can differ among cation sites, even when the cation is dehydrated. For instance, in the framework of X zeolite, the barrier for cation diffusion into supercages is lower than that for diffusion into sodalite cages and hexagonal prisms.⁷³ Furthermore, as indicated by eqn (13), changes in temperature have a more significant impact on the diffusion process when the activation energy is higher.

The exchange of two different cations is a more complex process, and the inter-diffusion coefficient D_{AB} does not directly follow the Arrhenius equation. The value of D_{AB} is related to both D_{AA} and D_{BB} . If there is no correlation between the fluxes other than the influence of the electrical potential gradient, the relationship can be expressed as follows:⁷⁹

$$D_{AB} = \frac{D_{AA}^* D_{BB}^* [b^2 c_B (\partial \ln \alpha_A / \partial \ln c_A) + a^2 c_A (\partial \ln \alpha_B / \partial \ln c_B)]}{a^2 c_A D_{AA}^* + b^2 c_B D_{BB}^*} \quad (14)$$

Where α_A and α_B are activities of cation A and B, respectively, and D_i^* is defined as:

$$D_i = D_i^* \frac{\partial \ln \alpha_i}{\partial \ln c_i} \quad (15)$$

It is important to note that the flux J_A in a system with two different cations cannot be simply described by Fick's laws. The cation diffusion process is affected by both concentration gradients and the electrical potential gradient throughout the crystal, which is explained by the Nernst-Planck equation:²²

$$J_A = -D_{AB} [\nabla c_A + (ac_A F/RT) \nabla V] \quad (16)$$

Where F is Faraday, and V is the electrical potential. Combining eqn (13)–(16), it can be qualitatively concluded that high temperatures may also speed up the exchanging process between the two types of cations.

During the ion exchange process, zeolite hydrolysis is also temperature-dependent. Higher temperatures can accelerate zeolite hydrolysis and amorphization for several reasons:³⁴

(1) The ionization constant of water (K_w) increases with temperature, leading to higher concentrations of hydronium and hydroxyl ions; for example, pK_w decreases from 14 at 20 °C to 12 at 100 °C.⁸⁰

(2) Elevated temperatures enhance the diffusion of incoming hydronium cations into zeolite.

(3) High temperature facilitates reactions involved in zeolite hydrolysis, including hydronium absorption and the breaking of Si–O and Al–O bonds.⁸¹

Nevertheless, the relationship between zeolite hydrolysis and temperature is not linear. Zeolites can remain stable in water within a specific temperature range. Buhl *et al.* investigated the hydrothermal stability of various ion-exchanged X zeolite samples at temperatures between 150 °C and 240 °C,⁸² comparing their water sorption capacities. Their findings revealed that Li^+ and Na^+ exchanged zeolites were hydrothermally stable below

200 °C, while K^+ , Rb^+ , Sr^{2+} , and Ba^{2+} exchanged zeolites experienced significant degradation above 170 °C. Ravenelle *et al.* assessed the hydrothermal stability of zeolites Y and ZSM-5 with varying Si/Al ratios.⁸³ They found that all ZSM-5 zeolites were stable at 200 °C in liquid water, but the micropore volumes of Y zeolites significantly decreased after being heated at 150 °C for 6 h in liquid water. It is challenging to accurately predict the breakdown temperatures of zeolites, as these temperatures mainly depend on the density of defects (silanols) in the zeolite, which are influenced by multiple factors including Si/Al ratios, the framework topologies, and synthesis and post-synthesis methods.⁸⁴

Therefore, it is crucial to balance the effects of temperature on the thermodynamics and kinetics of the ion exchange process with the hydrothermal stability of the zeolite. Typically, ion exchange temperatures are kept below 100 °C to avoid significant changes in the total concentration of cations. If the zeolite is stable at 100 °C in water, consideration should be given to the influence of temperature on the degree of ion exchange. Conversely, if the zeolite is not stable at this temperature, the ion exchange temperature should be reduced to ensure the stability of the zeolite.

7. Effect of ion exchange time

Ion exchange is a time-dependent process that does not occur instantaneously but instead requires time to reach equilibrium.⁸⁵ As shown in Fig. 11, the degree of ion exchange initially increases with time, eventually reaching an equilibrium where further cation loading in the zeolite cannot be enhanced by prolonging the ion exchange time.⁵⁴ As a type of adsorption, the kinetics of ion exchange can be modeled using adsorption kinetics models, especially the pseudo-first-order kinetic model and the pseudo-second-order model, which are widely used for liquid adsorption due to their effectiveness in curve fitting.⁸⁶ By applying these kinetic models, the relationship between cation loading and ion exchange time can be established, allowing for the prediction of the time needed to achieve ion exchange equilibrium.

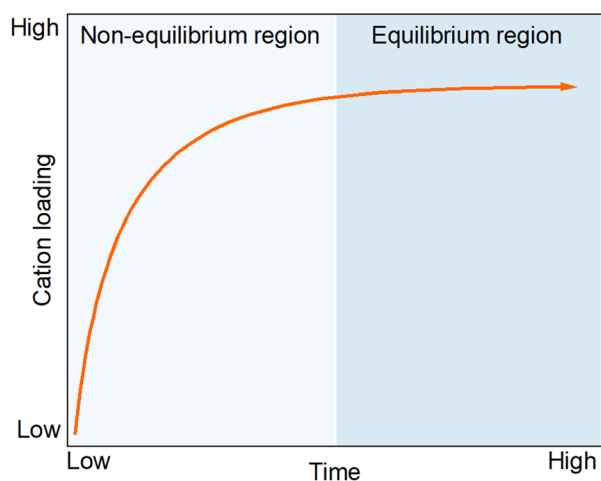


Fig. 11 Typical kinetic curve illustrating the relationship between cation loading and ion exchange time.

If incoming cations serve as the adsorption sites for the zeolite adsorbent, extending the ion exchange time can enhance the adsorption performance until ion exchange equilibrium is reached. After equilibrium, further increases in ion exchange time may not improve, and could even reduce, the adsorption properties. For instance, Song *et al.* studied Ag-exchanged zeolite Y for adsorptive desulfurization and found that the desulfurization rate significantly increased before peaking at 24 hours, then declined.⁵⁵ They suggested that Ag^+ loading increased with ion exchange time, enhancing performance, but an excessive Ag species could block zeolite pores after 24 hours, reducing desulfurization efficiency.⁵⁵ Similarly, Liu *et al.* investigated Zn-exchanged zeolite Y and identified an optimal ion exchange time of 4 hours for benzene purification.⁵⁷ They noted that excess Zn^{2+} might accumulate and block zeolite channels after 4 hours, resulting in a decrease in the adsorption selectivity to benzene.⁵⁷

Additionally, the impact of zeolite hydrolysis should not be overlooked. Sung *et al.* observed non-framework Al^{3+} ions in Ni-exchanged zeolite Y after prolonged ion exchange, which indicates structural hydrolysis and damage.⁴⁸ Firor and Seff also noted that excessive ion exchange time could lead to the disintegration of single crystals in zeolite A.⁵⁰

To minimize significant hydrolysis and the risk of pore blockage, the ion exchange time should be as brief as possible. Based on kinetic curves, it is advisable to separate zeolites from the ion exchange solution promptly as equilibrium approaches.

8. Effect of calcination temperature

After filtering and drying zeolites, the cations within them, especially those located in large cages, remain hydrated. Calcination aids in dehydrating these cations, exposing them to other adsorbates while altering their interactions with the zeolite framework and leading to cation migration. As the calcination temperature rises, the hydration levels of the cations decrease, resulting in more pronounced migration.

Generally, cations prefer to occupy crystallographic sites that maximize interactions with the framework oxygens and minimize electrostatic repulsion.¹¹ For instance, in the FAU-type zeolite, a commonly used zeolite employed for adsorption separation in industry,⁴ cation distribution can be summarized as follows.¹¹ In the FAU topological structure (Fig. 12⁸⁷), the six-membered rings (site I, I', II) contain more framework oxygens than the four-membered rings (site III, III'), resulting in the cations preferentially occupying the cation sites located in the former. Moreover, compared to the site I and I', the site II minimizes electrostatic repulsion between cations. Hence, in the absence of competition, most cations preferentially occupy site II. When site II approaches its maximum capacity of 32 per unit cell, sites I and I' become the next preferred locations. Except for K^+ and Ag^+ , it is impossible for the cations to simultaneously occupy both site I and I' within the same hexagonal prism due to strong repulsion from their close proximity. As the number of cations increases from 32 to 48 per unit cell, most cations prefer to occupy site I. When the

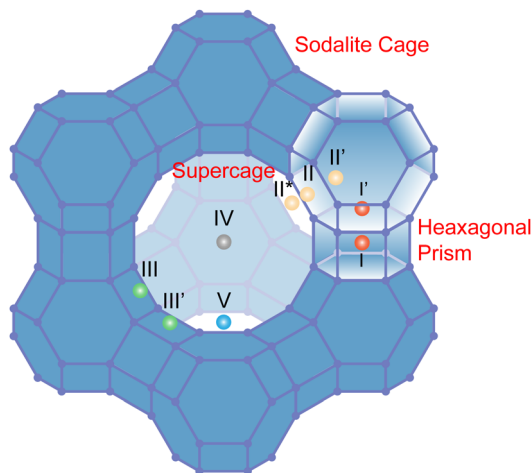


Fig. 12 Diagram of the FAU structure, illustrating the cation site designations. Site I: centre of hexagonal prism; site I': in the sodalite cage, near the hexagonal window adjacent to the hexagonal prism; site II: centre of the hexagonal window between the sodalite cage and the supercage; site II': within the sodalite cage, near the hexagonal window adjacent to the supercage; site II*: within the supercage, near the sodalite cage; site III: within the supercage, near a square window shared by the sodalite cage and the supercage; site III': within the supercage, near a square window between the hexagonal prism and the supercage; site IV: centre of the supercage; site V: centre of the 12-ring window shared by two supercages.

number of cations reaches between 48 and 64 per unit cell, occupation of site I decreases while that of site I' increases, because the hexagonal prism configuration allows one site I to effectively convert into two site I' to accommodate more cations. Once sites II and I' are filled up, other cation sites would be considered for occupation.

However, the above cation distribution changes when they are hydrated. Assuming the cations are initially dehydrated, water molecules diffusing into the supercages or sodalite cages can attract the cations, causing them to deviate from their original sites and become hydrated. Mortier *et al.* found that while the cation distribution of dehydrated NaY zeolite could not be significantly changed with increasing calcination temperature, the distribution of the hydrated cations could be.⁸⁸ Under a water pressure of 1870 Pa, Na⁺ cations preferentially migrated to site I', where they could interact more effectively with water molecules in sodalite cages, and this preference increased with the calcination temperature. Norby *et al.* indicated that the energy differences among various cation distributions in zeolite Cs(Na)-Y were minimal, and even weak interactions between the cations and adsorbed gases could alter these distribution.⁸⁹ Interestingly, the migration of Cs⁺, the largest cation, is hardly affected by kinetics, suggesting that the calcination primarily affects cation dehydration and migration. As the calcination temperature rises, cation migration becomes increasingly significant.⁹⁰

In multi-cycle ion exchange operations, calcining the zeolite after each ion exchange can indirectly boost the effectiveness of subsequent exchanges.⁹¹ Normally, the substitution of Na⁺ cations with Cs⁺ in NaY zeolite can reach a maximum of around 70% through ion exchange in aqueous cesium salt solutions at

room temperature.⁹² However, after calcination and dehydration, a portion of the residual Na⁺ cations can migrate to exchangeable sites, allowing for further enhancement of ion exchange capacity in subsequent cycles. Koller *et al.* reported that the cesium exchange levels in Cs(Na)-Y increased from 72% to 90% through a three-fold exchange-calcination cycle.⁹² Similarly, Norby *et al.* observed a similar phenomenon that cesium exchange levels in Cs(Na)-Y increased from 68% to 83% using the same method.⁸⁹

Furthermore, there exist structural changes in the zeolite frameworks during calcination. Notably, the framework of zeolite is flexible, which makes it impossible for the framework to remain unchanged during calcination.⁹³ In pure siliceous zeolite, where extra-framework cations are absent, the thermal expansion of zeolite is mainly influenced by the thermal vibrations of the framework oxygen atoms. These vibrations cause rotations of TO₄ tetrahedra (where T = Si), resulting in either positive or negative thermal expansion.⁹⁴ On the other hand, when the channels are filled with cations, which is common in zeolite adsorbents, these extra-framework cations can interact with the zeolite framework and control its thermal expansion.⁹⁵ During calcination, the hydrated cations undergo dehydration and migration, resulting in the adaptation of the zeolite framework to these migrations.⁹⁶ As the extra-framework cations become fully dehydrated, they can restrict the rotation of the TO₄ tetrahedra (where T = Si or Al), thereby mitigating structural changes in zeolites.^{97,98} However, if zeolite is calcined at excessively high temperatures, the extra-framework cations can no longer stabilize the framework. At high temperatures, T-O-T bonds will vibrate severely and even break, leading to zeolite structural collapse.⁹⁹ Because breaking the Si-O bond requires more energy than breaking the Al-O bond,¹⁰⁰ zeolite framework collapse is often accompanied by dealumination of the framework. The structural changes of hydrated zeolite during

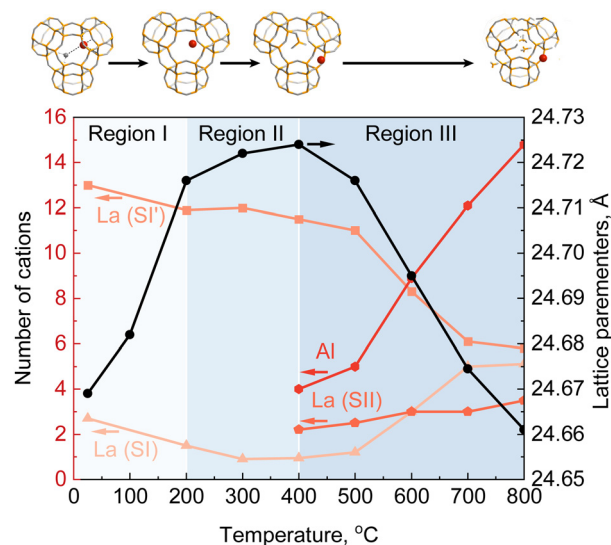


Fig. 13 Lattice parameter (●) of LaY zeolite and migration of La³⁺ and Al³⁺ extra-framework cations in LaY zeolite during heating.¹⁰¹ Region I: cation migration accompanied by dehydration; region II: complete migration of dehydrated cations; region III: collapse of the zeolite framework.

high-temperature calcination can be divided into three regions, as shown in Fig. 13:¹⁰¹

(1) Region I: extra-framework cations begin to migrate during dehydration, resulting in either positive or negative framework expansion depending on the cation rearrangement.

(2) Region II: extra-framework cations are almost fully dehydrated, and the distortions of the zeolite framework are restrained by the remaining cations.

(3) Region III: the zeolite framework starts to collapse, with some Al³⁺ cations leaving the framework, causing oxygen anions from the empty tetrahedra to be drawn to neighboring silicon tetrahedra, resulting in the zeolite contracting.

In some cases, zeolite may exhibit weak thermal stability, which can eliminate region II and lower the starting temperature of region III.⁹⁹ Moreover, when the extra-framework cations are too small to significantly impact the expansion of the zeolite framework, such as protons, region II will undergo apparent thermal expansion.¹⁰²

The thermal expansion of zeolite, resulting from the rearrangement of extra-framework cations, is unavoidable. The magnitude of this expansion depends on various factors such as the Si/Al ratio of the zeolite framework, the nature of charge-compensating cations, the coordination of bare cations, and the framework topology of the zeolite.¹⁰⁰ However, preventing the collapse of zeolite is achievable and should be a key focus. Each type of zeolite has a specific temperature at which significant structural collapse occurs; therefore, the calcination temperatures should not exceed this threshold.

9. Other effects

There are several other ion exchange factors that influence the adsorption properties of zeolites; yet research on these factors is limited, and their mechanisms remain unclear. These factors include the choice of precursor salt, the presence of acidic gases, and the volume-to-mass ratio of the solution to zeolite. To emphasize the importance of these factors, we review them in this section.

9.1 Precursor salt selection

When preparing an ion exchange solution, selecting the appropriate precursor is crucial. The choice of precursor can significantly impact the adsorption properties of the ion-exchanged zeolite. Sosa and Rios found that there were different degrees of ion exchange depending on the precursor salt used in the solution, which was likely due to the influence of anions on the pH of the solutions.¹⁰³ Lotfi *et al.* also agreed that anions could affect the degree of ion exchange and demonstrated through calculations that the formation energy of ion-exchanged zeolite was very sensitive to the type of salt.¹⁰⁴ Lima *et al.* exchanged sodium cations in NaX and NaA zeolites with cesium solutions made from three different cesium salts (chloride, nitrate, and acetate) and observed variations in cation distributions depending on the type of cesium salt used.¹⁰⁵ Young and Ki demonstrated that the adsorption

performance of zeolite was directly affected by precursor salts in ion exchange solutions.¹⁰⁶ They compared the adsorptive desulfurization performances of three Cu-Y zeolites exchanged with Cu(NO₃)₂, Cu(Ac)₂, and CuSO₄ respectively, and found that the zeolite exchanged with Cu(Ac)₂ exhibited the highest adsorption capacity. This was attributed to the impact of Cu precursors on the framework atoms (Al and Si) of zeolite, the positioning of Cu²⁺, and the extent of ion exchange. However, they didn't explain the mechanisms behind these differences.

Although there is some evidence proving that precursor selection affects cation exchange and zeolite adsorption, understanding the role of anions within the zeolite and their impact on cation exchange remains challenging. It is difficult to detect the extra-framework anions within the zeolite, and the role of the anions may depend on the nature of the cations. With the development of theoretical calculations, they can help us better understand the role of anions in ion exchange.¹⁰⁷

9.2 Presence of acidic gases

As mentioned earlier, zeolite hydrolysis results in an alkaline solution capable of absorbing acidic gases (*i.e.*, carbon dioxide) from the air.²² Prolonged exposure to these gases depletes hydroxyl ions, which promotes the reaction described in eqn (9) and further hydrolysis of zeolite.¹⁰⁸ Additionally, while some alkaline earth cations are soluble in alkaline solutions, their carbonates are not. The solubility of these carbonates is detailed in Table 1.¹⁰⁹ When a considerable amount of carbon dioxide is absorbed into the solution, even if the alkaline earth cations remain dissolved, their association with carbonate or bicarbonate ions can disrupt cation diffusion into zeolite.¹¹⁰ For example, in a solution in contact with NaX zeolite that had been exposed to air for an extended period, the total carbonate concentration was 2×10^{-4} M at a volume-to-mass ratio of 100.¹¹⁰ This concentration is significant, particularly considering that cation concentrations during zeolite preparation typically range around 10^{-1} M. However, there is a lack of research on how carbonates affect the adsorption performance of zeolites.

9.3 Volume-to-mass ratio of the solution to zeolite

When zeolite is added to a solution, the mass of the zeolite must be considered. Based on ion exchange isotherms, the degree of ion exchange may improve as the volume-to-mass ratio of the solution to zeolite increases. However, a higher solution volume does not always correlate with enhanced adsorption performance of the zeolite. Song *et al.* compared the desulfurization ratio of Ag-Y zeolites ion-exchanged with

Table 1 The solubility constants of three alkaline earth carbonates (25 °C). All data represent average values collected from the literature, as summarized in ref. 109

Carbonates	log K_s
CaCO ₃	-8.45
SrCO ₃	-9.27
BaCO ₃	-8.56

different solution volumes, ranging from 10 mL to 40 mL.⁵⁵ They found that the zeolite treated with 20 mL of solution demonstrated the best desulfurization performance. While a larger volume can facilitate greater cation loading, an excessive volume may block some zeolite pores.⁵⁵ Additionally, high solution volumes can dissolve more aluminum and silicon species, promoting zeolite hydrolysis. Thus, the adsorption capacity may initially increase with solution volume before eventually decreasing, indicating that an optimum solution volume exists, though few studies have explored this mechanism.

10. Conclusion and outlook

Given their exceptional performance in terms of environmental sustainability, efficiency, and cost-effectiveness, adsorptive separations based on zeolite adsorbents exhibit tremendous potential for further development. In order to enhance the selectivity of zeolite adsorption, ion exchange has been widely employed in the introduction of extra-framework cations into zeolite adsorbents. In this review, we provide a concise overview of the various factors impacting zeolite ion exchange and delve into the mechanisms by which these factors affect zeolite adsorption. Normally, zeolites with a high degree of ion exchange, proper cation distribution, and high surface area will exhibit remarkable selective adsorption properties. Hence, there are four criteria proposed to distinguish the mechanisms of ion exchange factors in zeolite adsorption, namely the degree of ion exchange, cation migration, the integrity of the zeolite framework, and pore blockage within the zeolite. To facilitate discussion, this review article primarily summarizes the relationships between these criteria and the critical factors in ion exchange. Based on these relationships, corresponding suggestions are provided to optimize the ion exchange processes.

Ion exchange in zeolite is a complex process consisting of cation hydration, diffusion, adsorption, and desorption, while it is sometimes disturbed by some side-reactions such as zeolite and cation hydrolysis, salt imbibition, and even carbon dioxide absorption. Despite the thermodynamic and kinetic data of the entire ion exchange process are measurable through experiments, it is challenging to identify the contribution of each component to the thermodynamics and kinetics, and to distinguish which component dominates the whole process. With the development of theoretical studies, it has been established that molecular simulation approaches can provide a deep understanding of the ion exchange process on a molecular and atomic scale,¹¹¹ which is not detectable through experimental approaches. For instance, Monte Carlo simulation has been successfully employed to elucidate the mechanisms of cation hydration affecting the equilibrium ion exchange properties in zeolite Y.¹¹² Therefore, further studies of molecular simulation should be utilized to gain deeper insights into the mechanism of ion exchange in zeolites at the molecular scale, thereby guiding us in better optimizing experimental operations.

Additionally, when we introduce more than one type of cation into zeolite, the complexity of the ion exchange system

will be multiplied, requiring more synergistic investigations combining experiment and theory. The utilization of polymetallic cation exchange in zeolite has been demonstrated to facilitate more precise control over pore size, internal electrostatic field, and adsorption sites compared to monometallic cation exchange.^{113,114} Nevertheless, it is challenging to achieve an optimal cation distribution and proportion in polymetallic cation-exchanged zeolites due to the varying preferences of various cation sites for specific cations and the complex equilibrium of multicomponent ion exchange. Thus, the combination of crystal structure analysis with molecular simulation deserves further study to determine the principles of cation distribution and ion exchange equilibria in polymetallic cation-exchanged zeolites.

Ultimately, we hope this article provides a thorough comprehension of the ion exchange factors affecting zeolite adsorption and aids in the exploration of zeolite adsorbents for specific chemical separations. During searching for suitable zeolite adsorbents for specific chemical separations, comparing the adsorption properties of different cation-exchanged zeolites is an essential method.^{115,116} However, improper ion exchange processes may cause us to overlook suitable zeolite adsorbents. With a deeper understanding of the preparation of cation-exchanged zeolite adsorbents, we believe that more advanced zeolite adsorbents will emerge, contributing to significant advancements in adsorption separation.

Data availability

No primary research results, software or code have been included and no new data were generated or analysed as part of this review.

Conflicts of interest

There are no conflicts to declare.

Acknowledgements

The authors greatly thank the National Natural Science Foundation of China (grant U23A20113, 22322803, 22178059 and 22408207), Qingyuan Innovation Laboratory (00523005, 00725001) for their financial supports.

References

- 1 D. S. Sholl and R. P. Lively, *Nature*, 2016, **532**, 435–437.
- 2 M. Rethinasabapathy, S. M. Ghoreishian, S.-K. Hwang, Y.-K. Han, C. Roh and Y. S. Huh, *Adv. Mater.*, 2023, **35**, 2301589.
- 3 N. Kaitwade, *Adsorbents market growth*, <https://www.futuremarketinsights.com/reports/global-adsorbents-market>, (accessed 12 December 2023, 2023).
- 4 J. Pérez-Pellitero and G. D. Pirngruber, in *New Developments in Adsorption/Separation of Small Molecules by*

- Zeolites*, ed. S. Valencia and F. Rey, Springer, Cham, Valencia, 1st edn, 2020, ch. 7, vol. 184, pp. 195–225.
- 5 R. Bai, X. Song, W. Yan and J. Yu, *Natl. Sci. Rev.*, 2022, **9**, nwac064.
 - 6 L. Liu and A. Corma, *Nat. Rev. Mater.*, 2020, **6**, 244–263.
 - 7 B. Yue, S. Liu, Y. Chai, G. Wu, N. Guan and L. Li, *J. Energy Chem.*, 2022, **71**, 288–303.
 - 8 M. S. A. Baksh, E. S. Kikkinides and R. T. Yang, *Sep. Sci. Technol.*, 1992, **27**, 277–294.
 - 9 Y. Yang, P. Bai and X. Guo, *Ind. Eng. Chem. Res.*, 2017, **56**, 14725–14753.
 - 10 E. Pérez-Botella, S. Valencia and F. Rey, *Chem. Rev.*, 2022, **122**, 17647–17695.
 - 11 T. Frising and P. Leflaive, *Microporous Mesoporous Mater.*, 2008, **114**, 27–63.
 - 12 X. Yang, F. E. Epie pang, Y. Liu and R. T. Yang, *Chem. Eng. Sci.*, 2018, **178**, 194–198.
 - 13 G. Sethia, R. S. Somani and H. C. Bajaj, *RSC Adv.*, 2015, **5**, 12773–12781.
 - 14 M. Fan, J. Sun, S. Bai and H. Panezai, *Microporous Mesoporous Mater.*, 2015, **202**, 44–49.
 - 15 J. Liao, W. Wang, Y. Xie, Y. Zhang, L. Chang and W. Bao, *Sep. Sci. Technol.*, 2012, **47**, 1880–1885.
 - 16 G. Sethia, R. S. Somani and H. C. Bajaj, *Ind. Eng. Chem. Res.*, 2014, **53**, 6807–6814.
 - 17 A. Goursot, V. Vasilyev and A. Arbuznikov, *J. Phys. Chem. B*, 1997, **101**, 6420–6428.
 - 18 D. Fu, Y. Park and M. E. Davis, *Angew. Chem., Int. Ed.*, 2022, **61**, e202112916.
 - 19 D. Fan, K. Qiao, S. Zhang, X. Chen, H. Wang, Y. Zhang, Y. Zhang, Y. Yang, F. Hu, Y. Wang, Z. Chen, F. Liang, D. Zhai, R. Kumar Marella and T. Yu, *Sep. Purif. Technol.*, 2024, **344**, 127315.
 - 20 J. Sebastian, S. A. Peter and R. V. Jasra, *Langmuir*, 2005, **21**, 11220–11225.
 - 21 H. Xia, Y. Hu, Q. Bao, J. Zhang, P. Sun, D. Liang, B. Wang, X. Qiao and X. Wang, *Microporous Mesoporous Mater.*, 2023, **350**, 112442.
 - 22 R. P. Townsend and E. N. Coker, in *Stud. Surf. Sci. Catal.*, ed. H. van Bekkum, E. M. Flanigen, P. A. Jacobs and J. C. Jansen, Elsevier, Amsterdam, 1st edn, 2001, ch. 11, vol. 137, pp. 467–524.
 - 23 H. P. Gregor, *J. Am. Chem. Soc.*, 1948, **70**, 1293.
 - 24 A. Dyer, in *Stud. Surf. Sci. Catal.*, ed. J. Čejka and H. van Bekkum, Elsevier, Amsterdam, 1st edn, 2005, ch. 9, vol. 157, pp. 181–204.
 - 25 H. S. Sherry and H. F. Walton, *J. Phys. Chem.*, 1967, **71**, 1457–1465.
 - 26 K. R. Franklin and R. P. Townsend, *J. Chem. Soc., Faraday Trans. 1*, 1988, **84**, 2755–2770.
 - 27 G. L. Gaines and H. C. Thomas, *J. Chem. Phys.*, 1953, **21**, 714–718.
 - 28 K. Stanciakova, B. Ensing, F. Göttl, R. E. Buló and B. M. Weckhuysen, *ACS Catal.*, 2019, **9**, 5119–5135.
 - 29 L. Camacho, S. Deng and R. R. Parra, *J. Hazard. Mater.*, 2010, **175**, 393–398.
 - 30 R. L. Hartman and H. S. Fogler, *Ind. Eng. Chem. Res.*, 2005, **44**, 7738–7745.
 - 31 R. L. Hartman and H. S. Fogler, *Langmuir*, 2007, **23**, 5477–5484.
 - 32 K. Valdiviés-Cruz, A. Lam and C. M. Zicovich-Wilson, *J. Phys. Chem. C*, 2017, **121**, 2652–2660.
 - 33 C. J. Heard, L. Grajciar, C. M. Rice, S. M. Pugh, P. Nachtigall, S. E. Ashbrook and R. E. Morris, *Nat. Commun.*, 2019, **10**, 4690.
 - 34 C. J. Heard, L. Grajciar, F. Uhlík, M. Shamzhy, M. Opanasenko, J. Čejka and P. Nachtigall, *Adv. Mater.*, 2020, **32**, 2003264.
 - 35 M. Jin, M. Liu, P. Nachtigall, L. Grajciar and C. J. Heard, *Chem. Mater.*, 2021, **33**, 9202–9212.
 - 36 D. Zhai, L. Zhao, Y. Liu, J. Xu, B. Shen and J. Gao, *Chem. Mater.*, 2014, **27**, 67–74.
 - 37 J. Sun, H. Fang, P. I. Ravikovitch and D. S. Sholl, *J. Phys. Chem. C*, 2020, **124**, 668–676.
 - 38 J. Cama, C. Ayora, X. Querol and J. Ganor, *Environ. Sci. Technol.*, 2005, **39**, 4871–4877.
 - 39 K. V. Ragnarsdóttir, *Geochim. Cosmochim. Acta*, 1993, **57**, 2439–2449.
 - 40 D. Drummond, A. De Jonge and L. V. C. Rees, in *Fundamentals and Applications of Ion Exchange*, ed. L. Liberti and J. R. Millar, Springer, Netherlands, Dordrecht, 1st edn, 1985, ch. 26, vol. 98, pp. 345–369.
 - 41 T. E. Cook, W. A. Cilley, A. C. Savitsky and B. H. Wiers, *Environ. Sci. Technol.*, 1982, **16**, 344–350.
 - 42 H. E. Allen, S. H. Cho and T. A. Neubecker, *Water Res.*, 1983, **17**, 1871–1879.
 - 43 M. Chen, S. Nong, Y. Zhao, M. S. Riaz, Y. Xiao, M. S. Molokeev and F. Huang, *Sci. Total Environ.*, 2020, **726**, 138535.
 - 44 N. Finish, P. Ramos, E. J. C. Borojovich, O. Zeiri, Y. Amar and M. Gottlieb, *J. Hazard. Mater.*, 2023, **457**, 131784.
 - 45 R. P. Townsend and R. Harjula, in *Post-Synthesis Modification I*, ed. H. G. Karge and J. Weitkamp, Springer Berlin Heidelberg, Berlin, Heidelberg, 1st edn, 2002, ch. 1, vol. 3, pp. 1–42.
 - 46 M. S. Berber-Mendoza, R. Leyva-Ramos, P. Alonso-Davila, J. Mendoza-Barron and P. E. Diaz-Flores, *J. Chem. Technol. Biotechnol.*, 2006, **81**, 966–973.
 - 47 M. Suzuki, K. Tsutsumi, H. Takahashi and Y. Saito, *Zeolites*, 1988, **8**, 381–386.
 - 48 S. M. Seo, D. J. Moon, J. An, H.-K. Jeong and W. T. Lim, *J. Phys. Chem. C*, 2016, **120**, 28563–28574.
 - 49 D. Bae and K. Seff, *Microporous Mesoporous Mater.*, 2000, **40**, 233–245.
 - 50 R. L. Firor and K. Seff, *J. Phys. Chem.*, 1978, **82**, 1650–1655.
 - 51 J. Zhang, R. Singh and P. A. Webley, *Microporous Mesoporous Mater.*, 2008, **111**, 478–487.
 - 52 N. D. Hutson and R. T. Yang, *AIChE J.*, 2000, **46**, 2305–2317.
 - 53 Y. Liu, J. Xu, L. Jin, Y. Fang and H. Hu, *Asia-Pac. J. Chem. Eng.*, 2009, **4**, 666–671.
 - 54 V. J. Inglezakis, *J. Colloid Interface Sci.*, 2005, **281**, 68–79.
 - 55 H. Song, B.-L. Jiang, H.-L. Song, Z.-S. Jin and X.-L. Sun, *Res. Chem. Intermed.*, 2015, **41**, 3837–3854.

- 56 N. Sue-aok, T. Srithanratana, K. Rangsrivatananon and S. Hengrasmee, *Appl. Surf. Sci.*, 2010, **256**, 3997–4002.
- 57 H. Liu, R. Kang, H. Zhou, X. Yang, Y. Tan, L. Ma, L. Ma and J. Li, *Microporous Mesoporous Mater.*, 2023, **348**, 112405.
- 58 I. C. Ostroski, M. A. S. D. Barros, E. A. Silva, J. H. Dantas, P. A. Arroyo and O. C. M. Lima, *J. Hazard. Mater.*, 2009, **161**, 1404–1412.
- 59 M. A. Al-Ghouti and D. A. Da'ana, *J. Hazard. Mater.*, 2020, **393**, 122383.
- 60 M. Á. Lobo-Recio, C. Rodrigues, T. Custódio Jeremias, F. R. Lapolli, I. Padilla and A. López-Delgado, *Chemosphere*, 2021, **267**, 128919.
- 61 L. Yang, M. Gao, T. Wei and T. Nagasaka, *J. Hazard. Mater.*, 2021, **424**, 127428.
- 62 I. Langmuir, *J. Am. Chem. Soc.*, 1916, **38**, 2221–2295.
- 63 H. Freundlich, *Trans. Faraday Soc.*, 1932, **28**, 195–201.
- 64 J. Perić, M. Trgo and N. Vukojević Medvidović, *Water Res.*, 2004, **38**, 1893–1899.
- 65 K. Y. Foo and B. H. Hameed, *Chem. Eng. J.*, 2010, **156**, 2–10.
- 66 H. S. Sherry, *J. Phys. Chem.*, 1966, **70**, 1158–1168.
- 67 H. S. Sherry, *J. Phys. Chem.*, 1968, **72**, 4086–4094.
- 68 R. P. Townsend, K. R. W. Franklin and J. F. O'Connor, *Adsorpt. Sci. Technol.*, 1984, **1**, 269–283.
- 69 S. E. Rodriguez-Cruz, R. A. Jockusch and E. R. Williams, *J. Am. Chem. Soc.*, 1999, **121**, 8898–8906.
- 70 L. V. C. Rees, *Annu. Rep. Prog. Chem., Sect. A: Gen. Phys. Inorg. Chem.*, 1970, **67**, 191–212.
- 71 M. A. S. D. Barros, P. A. Arroyo, E. F. Sousa-Aguiar and C. R. G. Tavares, *Adsorption*, 2004, **10**, 227–235.
- 72 L. Tagami, O. Aparecida, A. Santos, E. Falabella, P. A. Arroyo and M. A. Angélica, *Acta Sci.*, 2001, **23**, 1351–1357.
- 73 A. Dyer, R. B. Gettins and R. P. Townsend, *J. Inorg. Nucl. Chem.*, 1970, **32**, 2395–2400.
- 74 A. Dyer and R. P. Townsend, *J. Inorg. Nucl. Chem.*, 1973, **35**, 3001–3008.
- 75 A. Dyer and A. B. Ogden, *J. Inorg. Nucl. Chem.*, 1975, **37**, 2207–2210.
- 76 A. R. Dyer and S. A. I. Barri, *J. Inorg. Nucl. Chem.*, 1977, **39**, 1061–1063.
- 77 E. Hoinkis and H. Levi, *Z. Naturforsch.*, 1969, **24a**, 1784–1790.
- 78 S. Kumar and S. Jain, *J. Chem.*, 2013, **2013**, 957647.
- 79 N. Brooke and L. Rees, *Trans. Faraday Soc.*, 1968, **64**, 3383–3392.
- 80 T. S. Light and S. Licht, *Anal. Chem.*, 1987, **59**, 2327–2330.
- 81 M.-C. Silaghi, C. Chizallet, J. Sauer and P. Raybaud, *J. Catal.*, 2016, **339**, 242–255.
- 82 J.-C. Buhl, M. Gerstmann, W. Lutz and A. Ritzmann, *Z. Anorg. Allg. Chem.*, 2004, **630**, 604–608.
- 83 R. M. Ravenelle, F. Schüßler, A. D'Amico, N. Danilina, J. A. Bokhoven, J. A. Lercher, C. W. Jones and C. Sievers, *J. Phys. Chem. C*, 2010, **114**, 19582–19595.
- 84 L. Zhang, K. Chen, B. Chen, J. L. White and D. E. Resasco, *J. Am. Chem. Soc.*, 2015, **137**, 11810–11819.
- 85 H. Khanmohammadi, B. Bayati, J. Rahbar-Shahrouzi, A.-A. Babaluo and A. Ghorbani, *J. Environ. Chem. Eng.*, 2019, **7**, 103040.
- 86 K. L. Tan and B. H. Hameed, *J. Taiwan Inst. Chem. Eng.*, 2017, **74**, 25–48.
- 87 W. Li, Y. Chai, G. Wu and L. Li, *J. Phys. Chem. Lett.*, 2022, **13**, 11419–11429.
- 88 W. J. Mortier, E. Van den Bossche and J. B. Uytterhoeven, *Zeolites*, 1984, **4**, 41–44.
- 89 P. Norby, F. I. Poshni, A. F. Gualtieri, J. C. Hanson and C. P. Grey, *J. Phys. Chem. B*, 1998, **102**, 839–856.
- 90 O. A. Ponomareva, P. A. Kots, Y. G. Kolyagin, V. V. Chernyshev and I. I. Ivanova, *Russ. Chem. Bull.*, 2017, **66**, 2021–2027.
- 91 A. Dyer, R. Gettins and J. Brown, *J. Inorg. Nucl. Chem.*, 1970, **32**, 2389–2394.
- 92 H. Koller, B. Burger, A. M. Schneider, G. Engelhardt and J. Weitkamp, *Microporous Mater.*, 1995, **5**, 219–232.
- 93 N. Shi, Y. Song, X. Xing and J. Chen, *Coord. Chem. Rev.*, 2021, **449**, 214204.
- 94 L. Leardini, S. Quartieri, G. Vezzolini and R. Arletti, *Microporous Mesoporous Mater.*, 2015, **202**, 226–233.
- 95 G. Cametti and M. Giordani, *Sci. Rep.*, 2024, **14**, 23778.
- 96 T. Carey, A. Corma, F. Rey, C. C. Tang, J. A. Hriljac and P. A. Anderson, *Chem. Commun.*, 2012, **48**, 5829–5831.
- 97 T. Carey, C. C. Tang, J. A. Hriljac and P. A. Anderson, *Chem. Mater.*, 2014, **26**, 1561–1566.
- 98 V. R. Buragadda, L. Yu, F. G. Alabarse, A. Haidoux, C. Levelut, A. van der Lee, O. Cambon and J. Haines, *RSC Adv.*, 2013, **3**, 9911–9915.
- 99 D. L. Bish and J. W. Carey, *Rev. Mineral. Geochem.*, 2001, **45**, 403–452.
- 100 G. Cruciani, *J. Phys. Chem. Solids*, 2006, **67**, 1973–1994.
- 101 A. Dosen and B. A. Marinkovic, *Bull. Mater. Sci.*, 2019, **42**, 86.
- 102 G. Agostini, C. Lamberti, L. Palin, M. Milanese, N. Danilina, B. Xu, M. Janousch and J. A. van Bokhoven, *J. Am. Chem. Soc.*, 2010, **132**, 667–678.
- 103 I. Garcia-Sosa and M. Solache-Rios, *J. Radioanal. Nucl. Chem.*, 1999, **241**, 469–473.
- 104 L. Sellaoui, E. P. Hessou, M. Badawi, M. S. Netto, G. L. Dotto, L. F. O. Silva, F. Tielens, J. Ifthikar, A. Bonilla-Petriciolet and Z. Chen, *Chem. Eng. J.*, 2021, **420**, 127712.
- 105 E. J. Lima, I. A. Ibarra, M. A. Vera, V. H. Lara, P. Bosch and S. Bulbulian, *J. Phys. Chem. B*, 2004, **108**, 12103–12110.
- 106 Y. H. Cha and K. B. Lee, *Chem. Eng. J.*, 2023, **468**, 143461.
- 107 F. S. Wanyonyi, T. T. Fidelis, H. Louis, G. K. Mutua, F. Orata, L. Rhyman, P. Ramasami and A. M. S. Pembere, *J. Mol. Liq.*, 2022, **355**, 118913.
- 108 R. Harjula, J. Lehto, J. H. Pothuis, A. Dyer and R. P. Townsend, *J. Chem. Soc., Faraday Trans.*, 1993, **89**, 971–976.
- 109 P. L. Brown, C. Ekberg and A. V. Matyskin, *Geochim. Cosmochim. Acta*, 2019, **255**, 88–104.
- 110 R. Harjula, A. Dyer and R. P. Townsend, *J. Chem. Soc., Faraday Trans.*, 1993, **89**, 977–981.
- 111 V. Van Speybroeck, K. Hemelsoet, L. Joos, M. Waroquier, R. G. Bell and C. R. Catlow, *Chem. Soc. Rev.*, 2015, **44**, 7044–7111.

- 112 M. Jeffroy, A. Boutin and A. H. Fuchs, *J. Phys. Chem. B*, 2011, **115**, 15059–15066.
- 113 Y. Liu, Y. Wu, W. Liang, J. Peng, Z. Li, H. Wang, M. J. Janik and J. Xiao, *Chem. Eng. Sci.*, 2020, **220**, 115636.
- 114 S. Chen, M. Zhu, Y. Tang, Y. Fu, W. Li and B. Xiao, *J. Mater. Chem. A*, 2018, **6**, 19570–19583.
- 115 S. Liu, Y. Chen, B. Yue, C. Wang, B. Qin, Y. Chai, G. Wu, J. Li, X. Han, I. da-Silva, P. Manuel, S. J. Day, S. P. Thompson, N. Guan, S. Yang and L. Li, *Chemistry*, 2022, **28**, e202201659.
- 116 Y. Khabzina, C. Laroche, J. Perez-Pellitero and D. Farrusseng, *Phys. Chem. Chem. Phys.*, 2018, **20**, 23773–23782.